ACS OMEGA

http://pubs.acs.org/journal/acsodf

Article

Hydrothermal Synthesis of $K_2Ti_6O_{13}$ Nanotubes/Nanoparticles: A Photodegradation Study on Methylene Blue and Rhodamine B Dyes

Kiran Kenchappa Somashekharappa and Sampangi Venkatesh Lokesh*

Cite This: *ACS Omega* 2021, 6, 7248–7256

Read Online

ACCESS | Metrics & More | Article Recommendations | Supporting Information

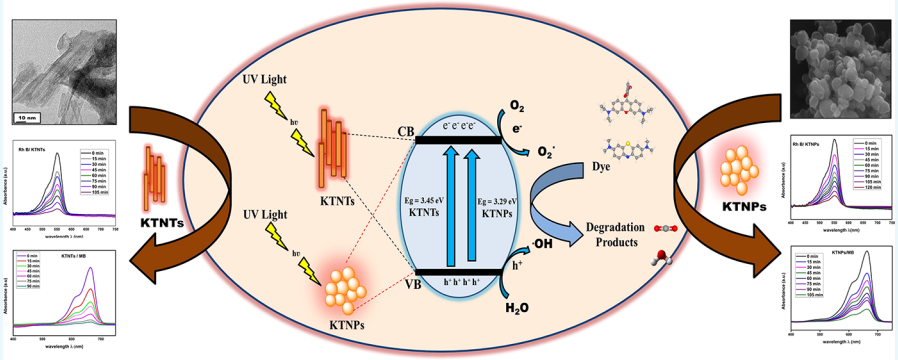

ABSTRACT: The degradation of methylene blue and rhodamine B dyes using potassium hexatitanate nanoparticles (KTNPs) and potassium hexatitanate nanotubes (KTNTs) synthesized via a hydrothermal method as efficient photocatalysts under UV light irradiation was investigated. The kinetics of degradation was determined for the two different catalysts——KTNPs and KTNTs——by monitoring the optical absorption of the dyes. The as-synthesized KTNPs were found to be spherical in shape with an average particle size of ∼36 ± 1.7 nm, whereas the KTNTs evidenced a tubular hollow structure with ∼7 nm internal diameter and ∼12 nm external diameter, as perused by structural and morphological studies. The larger surface area of KTNTs showed a greater impact on the photodegradation of dyes manifesting their high potential as compared to KTNPs under UV irradiation, and the reusability studies showed more than 90% (KTNTs) and 80% (KTNPs) degradation of the dyes even after the fourth cycle elucidating their stability.

1. INTRODUCTION

Water pollution has always been a major concern in the field of research in providing solutions to reduce its toxicological impact on human health and the environment. Synthetic dyes,[1−4] paints,[5] leather,[6] paper pulp,[7] printing,[8] fabric materials——textiles,[9] cosmetics,[10] and so on[11,12] are considered as the major sources of water pollution. The use of synthetic dyes is inexorable due to their wide range of applications owing to the fact that synthetic dyes are toxic, poorly biodegradable, and have hazardous characteristics causing the groundwater to pollute indelibly, further leading to health complications in humans and contamination of other water bodies.[13−15] The new insight toward restraining the plight is degradation of these synthetic dyes in a much efficient way, considering the factors such as low cost, more reliability, and biodegradability, with high stability and reusability.[16,17] Many researchers have emerged with their interests and have successfully reported a few techniques in this regard such as conventional coagulation,[18] chemical precipitation,[19] reduction,[20] adsorption,[21] ion exchange,[22] electrolysis,[23] impregnation,[24] reverse osmosis,[25] and photocatalytic degradation.[26−29] Considerably, adsorption and photocatalytic degradation are the most commonly used techniques by the researchers as rejoinders for the plight of water contamination, treating them as efficient, economic, and ecofriendly approaches. Methylene blue (MB) and rhodamine B (Rh B) dyes are commonly considered to mimic the wastewater, and many metal-oxide nanoparticles such as ZnO, TiO_2, SnO_2, Fe_2O_3, MgO, V_2O_5, and so on are generally employed as efficient sources in photocatalyst applications.[30−32]

Nanomaterials with one-dimensional structures such as nanotubes, nanoribbons, nanorods, nanowires, and nanobelts have gained prominence in the fields of photocatalysis,[33,34] photovoltaic cells,[35] lithium-ion batteries,[36] and supercapacitors.[37] The nanoparticles and nanotubes of potassium titanate are employed in the current research, and their study on photocatalytic applications is carried out owing to their high

Received: May 6, 2020
Accepted: March 1, 2021
Published: March 12, 2021

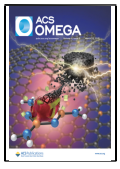

stability, low cost, and nontoxic nature. The synthesis of potassium titanate with a different morphology is reported by many researchers using various synthesis techniques such as calcination,[38] molten salt method,[39] anodization method,[40] sol–gel method,[41,42] and hydrothermal method.[40] We have employed the hydrothermal method for the synthesis of potassium hexatitanate nanotubes (KTNTs) and potassium hexatitanate nanoparticles (KTNPs); the hydrothermal method has the ability to synthesize large crystals with high quality, less impurities, and potential control over their composition and hence considered as one of the most promising tools for processing nanohybrids and nanocomposites.[43] Potassium hexatitanate is one among the novel materials and has fascinated the attention of researchers due to its high strength, thermal durability, stiffness, and aspect ratio characteristics.[44] This fibrous material is relatively economical and has been used in a wide range of applications and fields such as reinforcement materials for plastics, heat-insulating paints, friction modifiers for automotive brakes, and precision filters.[45,46] The chemical structure of potassium hexatitanate nanotubes ($K_2Ti_6O_{13}$) implies that the octahedral TiO_6 shares an edge at one level in a linear group of three, leading to the formation of a rectangular tunnel structure, as depicted in Figure 1.

2. MATERIALS AND METHODS

2.1. Chemicals. Titanium(IV) isopropoxide (97%), KOH (99.8%), NaOH (99.8%), H_2SO_4 (98%), ethanol (99%), and TiO_2 powder of anatase phase were procured from Sigma-Aldrich. MB dye (purity > 98%) and Rh B dye were purchased from Alfa Aesar and SD fine chemicals, respectively. All the chemicals were of analytical grade and used without any further purification. Deionized (DI) water used throughout the experiment was from Millipore Milli-Q Systems.

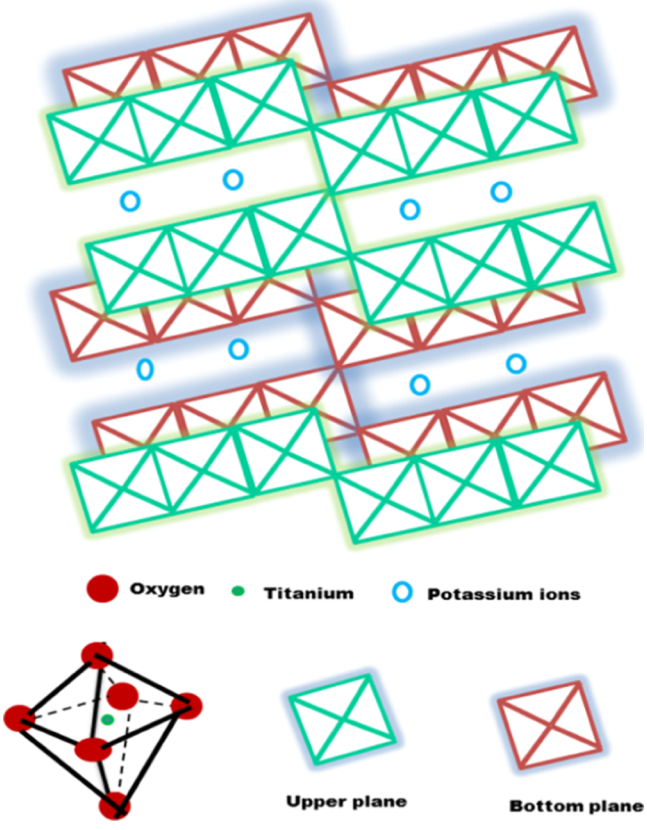

Figure 1. Crystal structure of potassium titanate ($K_2Ti_6O_{13}$) nanotubes.

2.2. Synthesis of Potassium Titanate Nanotubes/Nanoparticles. The synthesis procedure for both nanotubes and nanoparticles follows the same process flow as explained, omitting the reaction time (Figure 2). An aqueous solution of 10 M KOH was prepared by dissolving 14 g of potassium hydroxide flakes (precursor) in 25 mL of DI water under continuous stirring for 15 min using a magnetic stirrer. TiO_2 powder (0.8 g) was further added to the resultant solution under constant stirring for 30 min (800 rpm). The obtained solution was sonicated for 10 min and was then transferred to a 60 mL Teflon-lined stainless-steel autoclave and heated at 180 °C for 24 h (for nanotubes) and 180 °C for 12 h (for nanoparticles), maintaining the autoclave pressure (1 MPa). During the process, potassium hydroxide flakes react with TiO_2 powder, leading to the formation of potassium hexatitanate with water molecules (eq 1). The resultant product was thoroughly washed in ethanol, followed by DI water several times to obtain neutral pH, and further, the product was dried in a hot air oven for 10 h at 60 °C. Finally, the KTNTs/KTNPs so obtained were fine grinded using an agate mortar for 30 min, and the nanotube formation was confirmed by characterization, as discussed in further sections.

$$2KOH + 6TiO_2 \rightarrow K_2Ti_6O_{13} + H_2O \quad (1)$$

2.3. Characterization Techniques. The as-synthesized KTNTs/KTNPs were characterized using various analytical techniques, which highlight the crystal structure, functionality, size, shape, and morphology. Powder X-ray diffraction (XRD) was performed on a Rigaku Ultima IV diffractometer using Cu Kα radiation (λ = 0.15406 nm) in the 2θ range to overview the characteristic peak. Similarly, the size, shape, and morphology were evidenced using scanning electron microscopy (SEM) (Vega 3 Tescan) and transmission electron microscopy (TEM) (JEOL/JEM 2100). BET surface area analysis was performed on a BELSORP-mini II instrument. The functional groups and absorption spectra of the as-synthesized KTNTs/KTNPs were recorded using Fourier-transform infrared (FTIR) spectroscopy analysis (PerkinElmer Lambda 2) and UV–vis spectroscopy (PerkinElmer Lambda 750), respectively.

3. RESULTS AND DISCUSSION

3.1. Crystallographic Analysis. The XRD patterns of the as-synthesized KTNPs and KTNTs recorded reveal the monoclinic phase structure of $K_2Ti_6O_{13}$ with the $c2/m$ space group, having the lattice parameters a = 15.5 Å, b = 3.82 Å, c = 9.1 Å, and β = 99.5°, which is in good agreement with the JCPDS card number 74-0275 (Figure 3). The XRD patterns were recorded in the 2θ range of 10–70°, exploring the prominent peaks occurring along the (200), ($\bar{2}$01), (002), (203), (310), (112), (402), (403), ($\bar{4}$04), (602), (020), (022), (223), and ($\bar{7}$15) crystallographic planes, corresponding to the 2θ values of 11.34, 13.6, 19.52, 29.02, 29.7, 31.7, 32.72, 34.5, 42.3, 43.04, 47.6, 51.4, 57.2, and 67.3°. The data along with d-spacing and hkl planes are listed in Table 1. Similarly, the XRD patterns of the as-synthesized KTNPs and KTNTs after the photocatalytic degradation are recorded (for details, see Supporting Information Figure S2). The absence of unwanted peaks indicates the purity of the as-synthesized KTNTs/KTNPs, and their size was determined by Scherrer's formula, $D = 0.9\lambda/\beta\cos\theta$, where D corresponds to the crystalline size, λ is the X-ray wavelength, β is the full width at half-maximum of the diffraction

https://dx.doi.org/10.1021/acsomega.0c02087
ACS Omega 2021, 6, 7248–7256

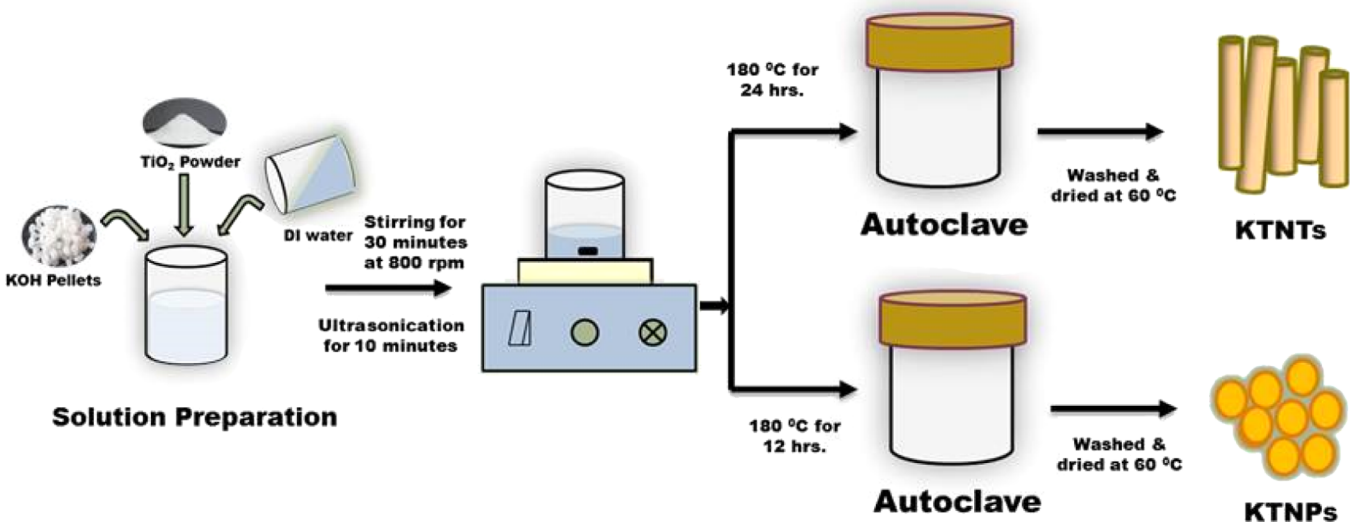

Figure 2. Schematic representation of the synthesis process flow of potassium titanate nanotubes.

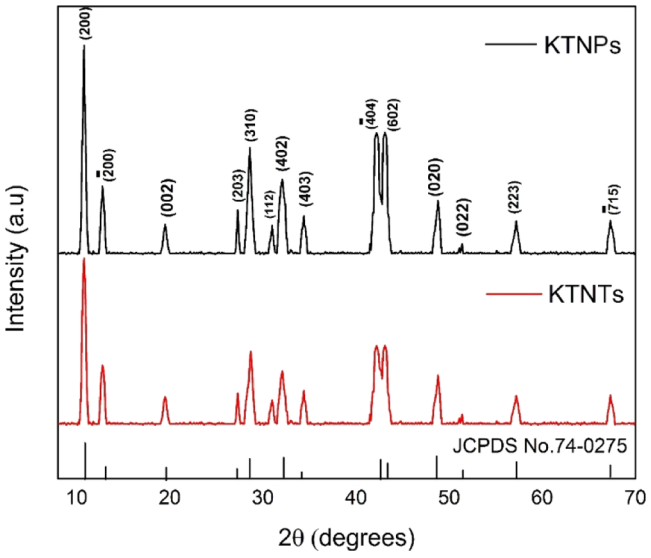

Figure 3. Intensity vs 2θ profile obtained for KTNTs/KTNPs revealing the monoclinic phase structure of $K_2Ti_6O_{13}$ with the $c2/m$ space group.

Table 1. Data Derived from the XRD Patterns Recorded for KTNTs/KTNPs

sl. no.	peak positions (2θ) in deg	crystallographic planes (hkl)	d (Å)
1	11.34	(200)	7.79
2	13.6	($\bar{2}$01)	6.506
3	19.52	(002)	4.547
4	29.02	(203)	3.077
5	29.7	(310)	3.009
6	31.7	(112)	2.818
7	32.72	(402)	2.711
8	34.5	(403)	2.643
9	42.3	($\bar{4}$04)	2.133
10	43.04	(602)	2.102
11	47.6	(020)	1.91
12	51.4	(022)	1.813
13	57.2	(223)	1.612
14	67.3	($\bar{7}$15)	1.39

peak, and θ is Bragg's diffraction angle. The average crystallite size of KTNPs was found to be ~32 nm and that of KTNTs was ~12 nm.

3.2. Elemental Composition and Morphological Analysis. The elemental composition of KTNPs and KTNTs was studied using energy-dispersive X-ray spectroscopy (EDAX), as depicted in Figure 4a,d, respectively. It is evident from the EDAX images and elemental data (inset) that the as-synthesized KTNPs and KTNTs are in the purest form without any additives due to the hydrothermal synthesis. The obtained KTNPs were in spherical shape, with an average particle size of ~36 ± 1.7 nm (for details, see Supporting Information Figure S1), and the SEM image of KTNTs clearly indicates the tubular structure formation from several dozens to hundreds of nanometers. Detailed studies on nanotubes were performed using TEM, which further confirmed the KTNTs with ~7 nm internal diameter and ~12 nm external diameter, as detailed in Figure 4g. We believe that the KTNT tubular formation is similar to that of earlier research reported which says that the formation of a 1D structure involves the dissolution of the 3D structure of TiO_2 by breaking the Ti−O−Ti bonds and rearranging the TiO_6 octahedra into 2D nanosheets further, so that the sheets could scroll or fold into a nanotubular morphology.[47]

3.3. Absorption/Transmittance Spectrum Analysis. The as-synthesized KTNPs and KTNTs were further studied by FTIR transmittance spectra analysis, which exhibited major peaks at 3465.3, 1640.4, 720.2, 500.1, and 464.6 cm^{-1} (Figure 5a). The peak at 500.1 cm^{-1} was from the crystal lattice vibration of TiO_6 octahedra and the peak at 1640.4 cm^{-1} was from the hydroxyl group, indicating the bending mode of water molecules adsorbed on the surface of KTNPs and KTNTs. The appearance of a broad peak at 3465.3 cm^{-1} corresponds to the O−H stretch of the surface hydroxyl groups on KTNPs and KTNTs. The typical FTIR absorption bands of potassium hexatitanate nanotubes were observed at 464.6 and 720.2 cm^{-1} due to Ti−O stretching and O−Ti−O bending vibrations of TiO_6 octahedra.[48] The as-synthesized KTNPs and KTNTs were further characterized by UV−vis diffuse reflectance spectroscopy (Figure 5b) to analyze the optical response property.[49] The absorption spectra of the as-synthesized KTNPs and KTNTs were found around 330 nm, and the derived data were further

https://dx.doi.org/10.1021/acsomega.0c02087
ACS Omega 2021, 6, 7248−7256

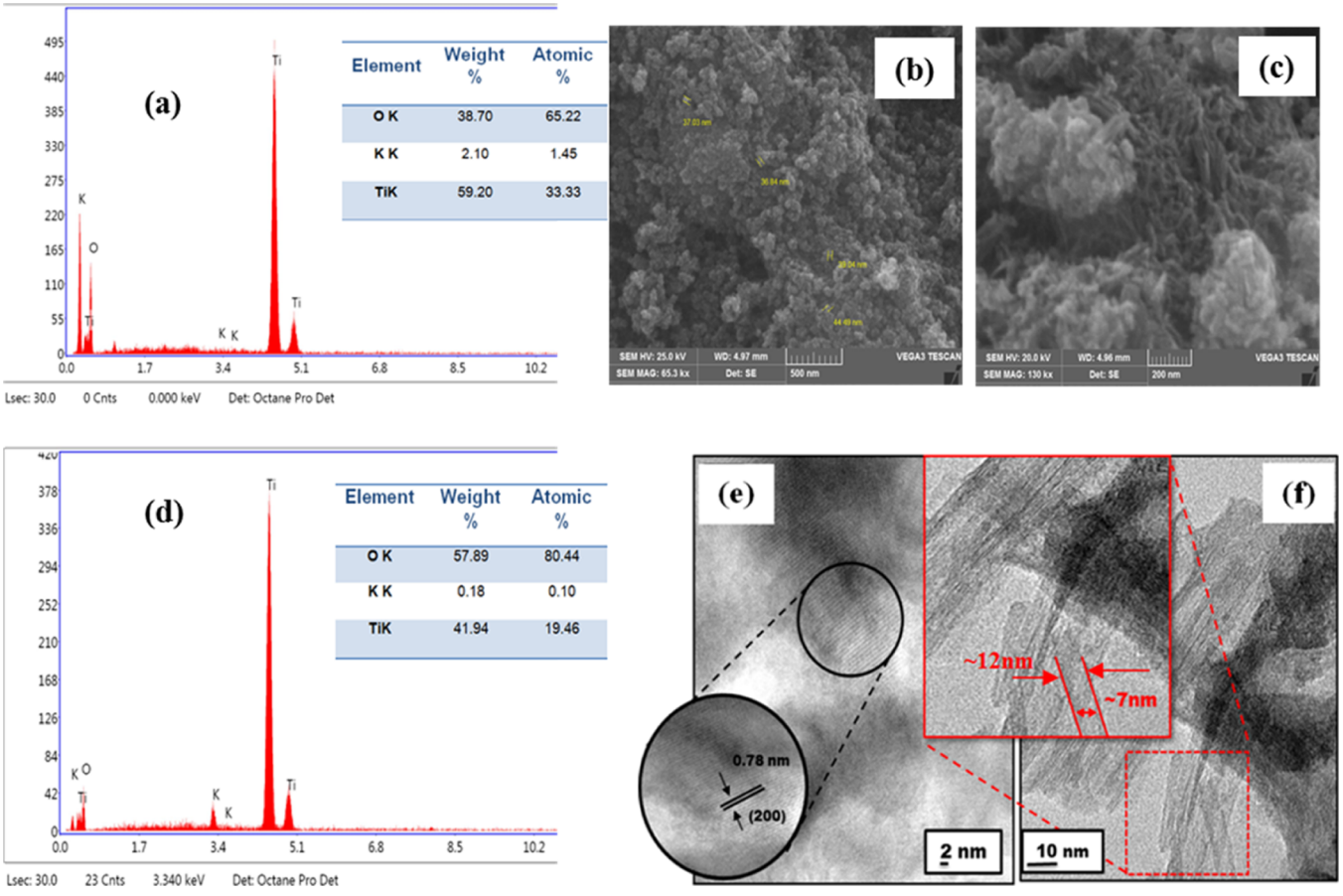

Figure 4. EDAX profile: (a,d) as-synthesized KTNPs and KTNTs with elemental analysis (inset), respectively. SEM images: (b,c) as-synthesized KTNPs and KTNTs, respectively. TEM images: (e) *d*-spacing of the (200) crystallographic planes of the monoclinic structure of KTNTs and (f) as-synthesized KTNTs with magnifications of 2 and 10 nm, respectively.

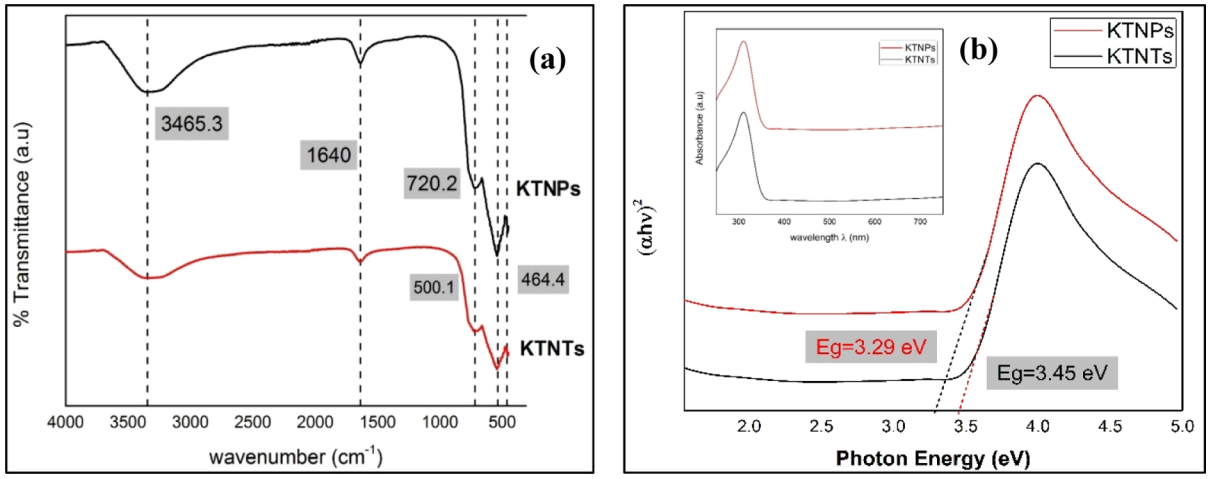

Figure 5. (a) FTIR transmittance spectra and (b) band gap determination from the UV−vis absorption spectra (inset) of the as-synthesized KTNPs and KTNTs.

used to calculate the optical band gap (E_g) from Tauc's relation.[50] A plot of $(\alpha h\nu)^2$ vs photon energy (eV) shows an intermediate linear region, and the extrapolation of the linear part can be used to calculate E_g from the intersection with the photon energy axis. The resultant E_g values for KTNPs and KTNTs calculated were found to be 3.29 and 3.45 eV, respectively.

3.4. Photodegradation Studies. The photocatalytic activity of the as-synthesized KTNPs and KTNTs was studied on MB and Rh B under UV irradiation (Figure 6). Initially, about 30 mg of catalysts was weighed and added into the dye solutions (MB and Rh B separately) of 10 ppm concentration; the mixtures were further stirred under dark conditions for 30 min to achieve the adsorption−desorption equilibrium before being exposed to UV irradiation (room temperature). The

https://dx.doi.org/10.1021/acsomega.0c02087
ACS Omega 2021, 6, 7248−7256

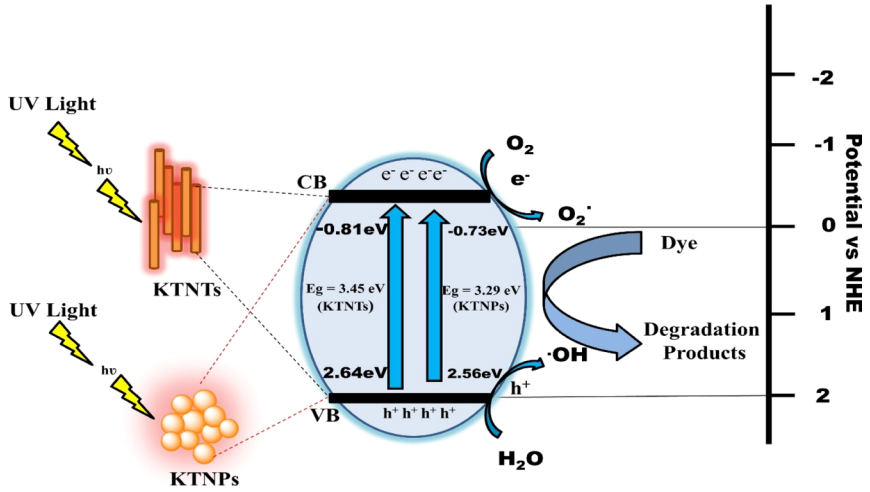

Figure 6. Schematic representation of the photocatalytic activity of KTNTs/KTNPs.

changes in the concentration of the dye solution were continuously monitored using a UV−vis spectrophotometer at 664 nm corresponding to the λ_{max} value of MB and 550 nm corresponding to the λ_{max} value of Rh B solutions by withdrawing samples for every 15 min interval and analyzed. Photocatalytic study was conducted after the adsorption−desorption equilibrium (dark condition) which was achieved using UV light irradiation. The removal of MB and Rh B dyes and the pseudo-first-order rate constants were calculated using eqs 2 and 3, respectively

$$\text{percentage of removal of dyes} = \frac{C_0 - C_t}{C_0} \times 100\% \quad (2)$$

$$\ln\left(\frac{C_0}{C_t}\right) = -kt, \qquad k = \text{rate constant } (\text{min}^{-1}) \quad (3)$$

where C_t and C_0 are the concentrations of MB and Rh B dyes at time $(t, 0)$, respectively.

The energy band gaps of valence band (E_{VB}) and conduction band (E_{CB}) were calculated by using the equation[51]

$$E_{VB} = \chi_{KTNTs/KTNPs} - E_o + 1/2E_g \quad (4)$$

$$E_{CB} = E_{VB} - E_g \quad (5)$$

The predictable mechanism[52] from the results obtained for the photocatalytic degradation of MB and Rh B dyes by $K_2Ti_6O_{13}$ nanostructures under UV irradiation can be elucidated as follows:

$$K_2Ti_6O_{13} + h\nu \rightarrow K_2Ti_6O_{13}(e^-_{(CB)} + h^+_{(VB)}) \quad (6)$$

$$O_2 + e^- \rightarrow {}^\bullet O_2^- \quad (7)$$

$$H_2O + h^+ \rightarrow {}^-OH + H^+ \quad (8)$$

$$^-OH + h^+ \rightarrow {}^\bullet OH \quad (9)$$

$$^\bullet O_2 + H^+ \rightarrow {}^\bullet HO_2 \quad (10)$$

$$dye + h\nu \rightarrow dye^\bullet \quad (11)$$

$$dye^\bullet + K_2Ti_6O_{13} \rightarrow dye + K_2Ti_6O_{13}e^-_{(CB)} \quad (12)$$

$$K_2Ti_6O_{13}e^-_{(CB)} + O_2 \rightarrow K_2Ti_6O_{13} + O_2^- \quad (13)$$

$$K_2Ti_6O_{13}e^-_{(CB)} + {}^\bullet O_2^- + 2H^+ \rightarrow K_2Ti_6O_{13} + H_2O_2 \quad (14)$$

$$K_2Ti_6O_{13}e^-_{(CB)} + H_2O_2 \rightarrow K_2Ti_6O_{13} + {}^\bullet OH + {}^-OH \quad (15)$$

$$dye^\bullet + O_2/{}^\bullet O_2^-/h^+_{(VB)} \rightarrow \text{degradation products} \quad (16)$$

The percentage of degradation for MB dye under UV irradiation on the catalysts KTNPs and KTNTs was 79.23% (105 min) and 82.06% (90 min), whereas it was found to be 77.54% (120 min) and 79.2% (105 min) for Rh B dye, respectively. The high degradation percentage of dyes denotes the high efficiency of the catalysts to produce photo-excited charges (e^- and h^+), which can be ascribed to the larger surface area and smaller particle size of the catalysts (Figure 9). The KTNTs have a higher degradation percentage, proving to be high-efficiency catalysts as compared to KTNPs (Figure 7).

3.5. Trapping Experiments. The proposed photocatalytic degradation mechanism is assessed by the active species by using quenchers such as acetic acid, and methanol for $^\bullet OH$ and h^+ radicals under UV light; the radical scavenging experiments for MB and Rh D dye degradation over KTNPs and KTNTs were performed (Figure 8a,b).

The rate of degradation of dyes was more when acetic acid was added and less with methanol addition (Figure 8b). Methanol acts as an h^+ ion quencher, so the reaction proceeds faster in the presence of h^+ ions than $^\bullet OH$.

3.6. BET Surface Area Analysis. The BET specific surface areas of KTNPs and KTNTs are calculated as 9.6 and 20 $m^2\ g^{-1}$, respectively (Figure 9). One-dimensional KTNTs have a larger surface area compared to zero-dimensional KTNPs which have a larger surface area and smaller particle size. This exhibits the more active sites, and hence KTNTs have a higher photocatalytic degradation property than the KTNPs.

3.7. Reusability Study. The reusability study on the as-synthesized KTNPs and KTNTs was carried out to determine the efficiency of the catalyst by exposing the catalysts for a number of runs and calculating the degradation percentage. During the fourth cycle, the catalyst removed approximately 90% of the KTNTs (Figure 10b) and 80% of KTNPs. The photodegradation efficiency of the KTNTs was further improved after cleaning with ethanol, followed by DI water ultrasonically, whereas that of KTNPs remains the same.

https://dx.doi.org/10.1021/acsomega.0c02087
ACS Omega 2021, 6, 7248−7256

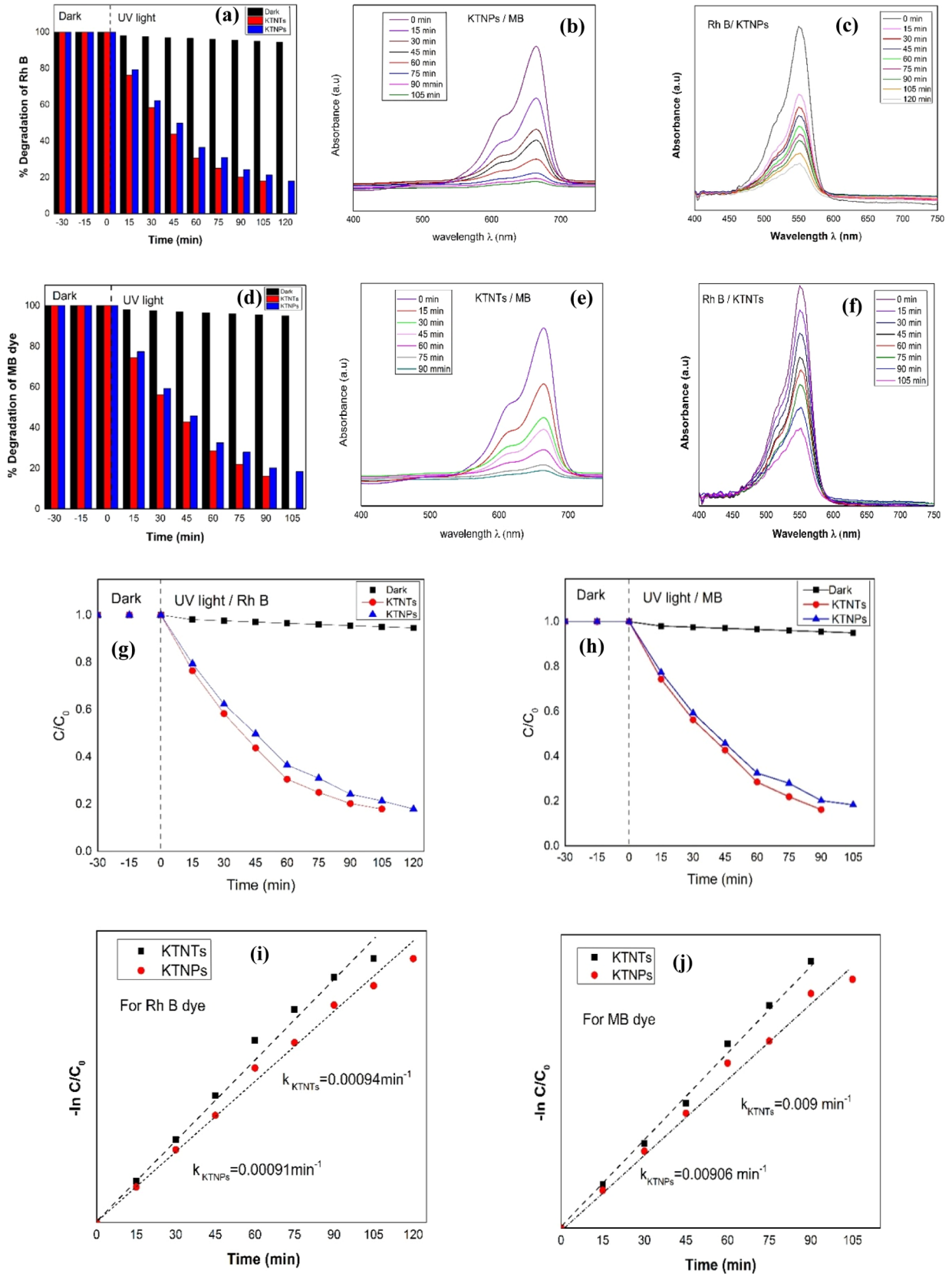

Figure 7. (a,d) Percentage degradation vs time (min); (b,c,e,f) absorbance vs wavelength (nm); (g,h) photocatalytic activity plot of C/C_0 vs irradiation time (min); and (i,j) rate constant of the photocatalytic activity.

Furthermore, the photocatalytic efficiency exhibited no major loss even after four cycles, and only a slight decrease in photodegradation efficiency was observed over a time period, indicating the better relative stability of the as-synthesized KTNTs, and during the process, the catalyst was not photo-corroded, highlighting the fair corrosion resistance property.

https://dx.doi.org/10.1021/acsomega.0c02087
ACS Omega 2021, 6, 7248−7256

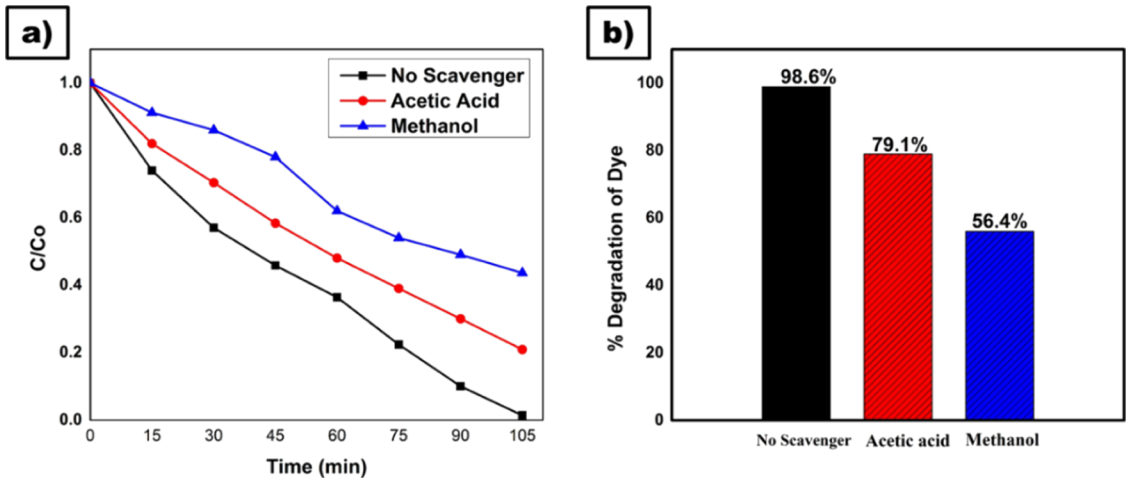

Figure 8. Trapping experiment plot (a). Concentration C/C_0 vs time (min) (b). Percentage degradation of dye vs scavengers.

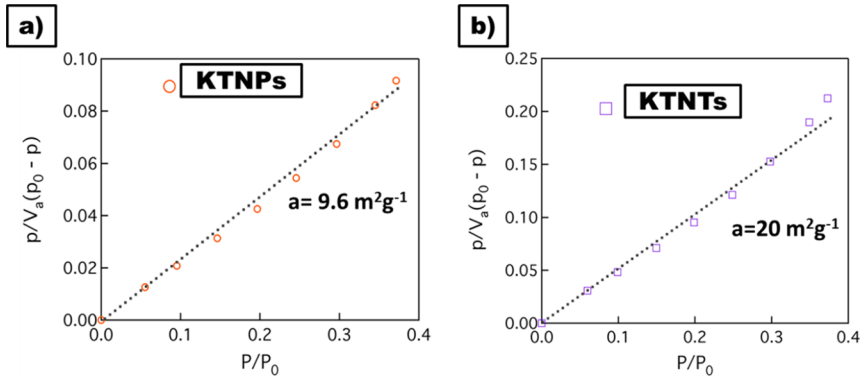

Figure 9. BET surface area plots: relative pressure P/P_0 vs $P/V_a(P_0 - P)$ of (a) KTNPs and (b) KTNTs.

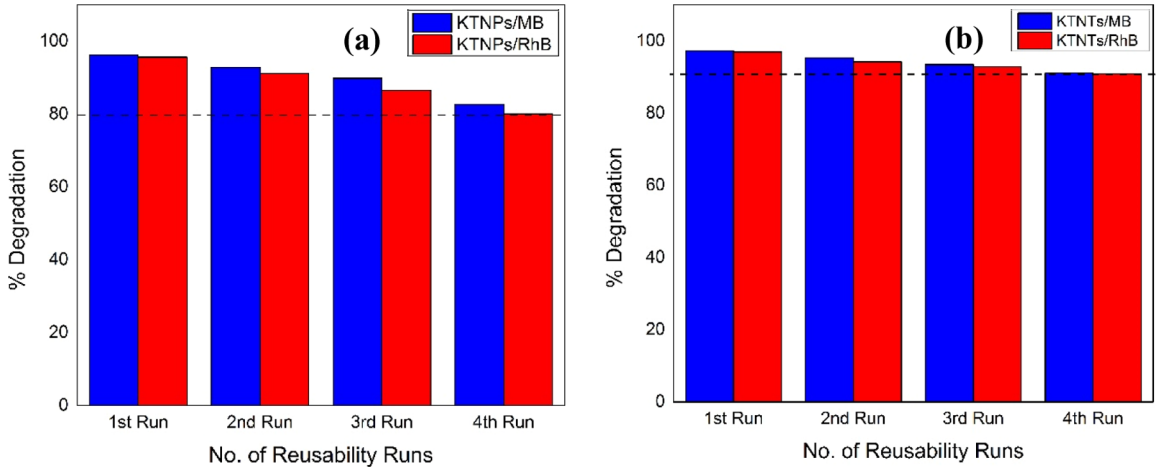

Figure 10. Plot of percentage degradation vs number of reusability runs of (a) KTNPs and (b) KTNTs.

The stability of the photocatalysts KTNPs and KTNTs was further confirmed after the photocatalytic degradation by UV–vis DRS (for details, see Supporting Information Figure S3b).

4. CONCLUSIONS

The kinetics of degradation was studied on hydrothermally synthesized KTNPs and KTNTs by tracking the optical absorption of the dyes (MB and Rh B). The as-synthesized KTNPs exhibited a spherical shape with an average particle size of ~36 ± 1.7 nm, whereas KTNTs revealed a tubular hollow structure with ~7 nm internal diameter and ~12 nm external diameter, as perused by the structural and morphological studies. The photodegradation study under UV irradiation confirms the higher efficiency of KTNTs as compared to KTNPs for both dyes owing to the fact that the large surface area and smaller particle size have a greater impact toward the photocatalytic activity. In addition, the reusability test on the catalysts elucidates that the KTNTs (90%) can be easily recovered with greater consistency even after the fourth cycle (MB and Rh B) and reused as compared to KTNPs (80%).

https://dx.doi.org/10.1021/acsomega.0c02087
ACS Omega 2021, 6, 7248−7256

Factors such as enhanced photocatalytic activity, greater photoabsorption efficiency, and reusability of KTNTs are promising in fostering catalytic reinforcement and their use in novel optic materials.

■ ASSOCIATED CONTENT

Supporting Information

The Supporting Information is available free of charge at https://pubs.acs.org/doi/10.1021/acsomega.0c02087.

Particle size analyzer data of KTNPs; XRD patterns of KTNPs and KTNTs after the photocatalytic degradation; UV−vis DRS spectra; and band gap calculation from Tauc's plot $(\alpha h\nu)^2$ versus photon energy (eV) of KTNPs and KTNTs after the photocatalytic degradation (PDF)

■ AUTHOR INFORMATION

Corresponding Author

Sampangi Venkatesh Lokesh − *Department of Nanotechnology, Centre for PG Studies-Bangalore Region, Visvesvaraya Technological University, Chikkaballapura 562101, India;* orcid.org/0000-0001-8666-4286; Email: lokeshsampangi@gmail.com

Author

Kiran Kenchappa Somashekharappa − *Department of Nanotechnology, Centre for PG Studies-Bangalore Region, Visvesvaraya Technological University, Chikkaballapura 562101, India;* orcid.org/0000-0002-1031-3583

Complete contact information is available at: https://pubs.acs.org/10.1021/acsomega.0c02087

Notes

The authors declare no competing financial interest.

■ ACKNOWLEDGMENTS

The authors are thankful to the financial support given by DST-SERB, Government of India, file no. SB/EMEQ-171/2014, to carry out the experiments.

■ REFERENCES

(1) Kim, Y.; McCoy, L. T.; Lee, E.; Lee, H.; Saremi, R.; Feit, C.; Hardin, I. R.; Sharma, S.; Mani, S.; Minko, S. Environmentally Sound Textile Dyeing Technology with Nanofibrillated Cellulose. *Green Chem.* **2017**, *19*, 4031−4035.

(2) Fukuzumi, S.; Ohkubo, K. Organic Synthetic Transformations Using Organic Dyes as Photoredox Catalysts. *Org. Biomol. Chem.* **2014**, *12*, 6059−6071.

(3) Grimm, J. B.; Brown, T. A.; Tkachuk, A. N.; Lavis, L. D. General Synthetic Method for Si-Fluoresceins and Si-Rhodamines. *ACS Cent. Sci.* **2017**, *3*, 975−985.

(4) Forgacs, E.; Cserháti, T.; Oros, G. Removal of Synthetic Dyes from Wastewaters: A Review. *Environ. Int.* **2004**, *30*, 953−971.

(5) Ali, I. New Generation Adsorbents for Water Treatment. *Chem. Rev.* **2012**, *112*, 5073−5091.

(6) Chowdhury, M.; Mostafa, M. G.; Biswas, T. K.; Mandal, A.; Saha, A. K. Characterization of the Effluents from Leather Processing Industries. *Environ. Processes* **2015**, *2*, 173−187.

(7) Mackay, D. M.; Roberts, P. V.; Cherry, J. A. Transport of Organic Contaminants in Groundwater. *Environ. Sci. Technol.* **1985**, *19*, 384−392.

(8) Mon, M.; Bruno, R.; Ferrando-Soria, J.; Armentano, D.; Pardo, E. Metal-organic framework technologies for water remediation: towards a sustainable ecosystem. *J. Mater. Chem. A* **2018**, *6*, 4912−4947.

(9) Lellis, B.; Fávaro-Polonio, C. Z.; Pamphile, J. A.; Polonio, J. C. Effects of Textile Dyes on Health and the Environment and Bioremediation Potential of Living Organisms. *Biotechnol. Res. Innov.* **2019**, *3*, 275−290.

(10) Sui, Q.; Cao, X.; Lu, S.; Zhao, W.; Qiu, Z.; Yu, G. Occurrence, Sources and Fate of Pharmaceuticals and Personal Care Products in the Groundwater: A Review. *Emerg. Contam.* **2015**, *1*, 14−24.

(11) Burri, N. M.; Weatherl, R.; Moeck, C.; Schirmer, M. A Review of Threats to Groundwater Quality in the Anthropocene. *Sci. Total Environ.* **2019**, *684*, 136−154.

(12) Edmunds, W. M.; Ahmed, K. M.; Whitehead, P. G. A review of arsenic and its impacts in groundwater of the Ganges-Brahmaputra-Meghna delta, Bangladesh. *Environ. Sci.: Processes Impacts* **2015**, *17*, 1032−1046.

(13) Routoula, E.; Patwardhan, S. V. Degradation of Anthraquinone Dyes from Effluents: A Review Focusing on Enzymatic Dye Degradation with Industrial Potential. *Environ. Sci. Technol.* **2020**, *54*, 647−664.

(14) Rasheed, T.; Bilal, M.; Nabeel, F.; Adeel, M.; Iqbal, H. M. N. Environmentally-Related Contaminants of High Concern: Potential Sources and Analytical Modalities for Detection, Quantification, and Treatment. *Environ. Int.* **2019**, *122*, 52−66.

(15) Tkaczyk, A.; Mitrowska, K.; Posyniak, A. Synthetic Organic Dyes as Contaminants of the Aquatic Environment and Their Implications for Ecosystems: A Review. *Sci. Total Environ.* **2020**, *717*, 137222.

(16) Benkhaya, S.; M'rabet, S.; El Harfi, A. A Review on Classifications, Recent Synthesis and Applications of Textile Dyes. *Inorg. Chem. Commun.* **2020**, *115*, 107891.

(17) Ahmad, A.; Mohd-Setapar, S. H.; Chuong, C. S.; Khatoon, A.; Wani, W. A.; Kumar, R.; Rafatullah, M. Recent Advances in New Generation Dye Removal Technologies: Novel Search for Approaches to Reprocess Wastewater. *RSC Adv.* **2015**, *5*, 30801−30818.

(18) Ryan, D. R.; McNamara, P. J.; Mayer, B. K. Iron-Electrocoagulation as a Disinfection Byproduct Control Strategy for Drinking Water Treatment. *Environ. Sci.: Water Res. Technol.* **2020**, *6*, 1116−1124.

(19) Matlock, M. M.; Howerton, B. S.; Atwood, D. A. Chemical Precipitation of Lead from Lead Battery Recycling Plant Wastewater. *Ind. Eng. Chem. Res.* **2002**, *41*, 1579−1582.

(20) Paramesh, C. C.; Halligudra, G.; Muniyappa, M.; Shetty, M.; Somashekharappa, K. K.; Rangappa, D.; Rangappa, K. S.; Shivaramu, P. D. Silver nanoparticles anchored TiO2 nanotubes prepared using saponin extract as heterogeneous and recyclable catalysts for reduction of dyes. *Ceram. Int.* **2020**, DOI: 10.1016/j.ceramint.2020.11.173.

(21) Le Cloirec, P.; Brasquet, C.; Subrenat, E. Adsorption onto Fibrous Activated Carbon: Applications to Water Treatment. *Energy Fuels* **1997**, *11*, 331−336.

(22) Nalaparaju, A.; Jiang, J. Ion Exchange in Metal-Organic Framework for Water Purification: Insight from Molecular Simulation. *J. Phys. Chem. C* **2012**, *116*, 6925−6931.

(23) Guo, M.; Feng, L.; Liu, Y.; Zhang, L. Electrochemical Simultaneous Denitrification and Removal of Phosphorus from the Effluent of a Municipal Wastewater Treatment Plant Using Cheap Metal Electrodes. *Environ. Sci.: Water Res. Technol.* **2020**, *6*, 1095−1105.

(24) Zhao, S.; Huang, K.; Lin, H. Impregnated Membranes for Water Purification Using Forward Osmosis. *Ind. Eng. Chem. Res.* **2015**, *54*, 12354−12366.

(25) Liu, C.; Guo, Y.; Zhang, J.; Tian, B.; Lin, O.; Liu, Y.; Zhang, C. Tailor-Made High-Performance Reverse Osmosis Membranes by Surface Fixation of Hydrophilic Macromolecules for Wastewater Treatment. *RSC Adv.* **2019**, *9*, 17766−17777.

(26) Hora, P. I.; Novak, P. J.; Arnold, W. A. Photodegradation of Pharmaceutical Compounds in Partially Nitritated Wastewater during UV Irradiation. *Environ. Sci.: Water Res. Technol.* **2019**, *5*, 897−909.

(27) Kiran, K. S.; Narayana, A.; Lokesh, S. V. Synthesis of SrTiO3 Nanotubes from Green TiO2 Nanoparticles for Enhanced Photocatalytic Activity. *Asian J. Chem.* **2020**, *32*, 2520−2528.

(28) Guo, S.-q.; Zhu, X.-h.; Zhang, H.-j.; Gu, B.-c.; Chen, W.; Liu, L.; Alvarez, P. J. J. Improving Photocatalytic Water Treatment through Nanocrystal Engineering: Mesoporous Nanosheet-Assembled 3D BiOCl Hierarchical Nanostructures That Induce Unprecedented Large Vacancies. *Environ. Sci. Technol.* **2018**, *52*, 6872−6880.
(29) Babu, J.; Muniyappa, M.; Rani, N.; Sabbanahalli, C.; Shetty, M.; Mudike, R.; Chitrabanu, C. P.; Shivaramu, P. D.; Nagaraju, G.; Rangappa, K. S.; S, A. K. C.; Rangappa, D. Carbon-Based TiO 2-x Heterostructure Nanocomposites for Enhanced Photocatalytic Degradation of Dye Molecules. *Ceram. Int.* **2021**, *47*, 10314−10321.
(30) Sudha, D.; Sivakumar, P. Review on the Photocatalytic Activity of Various Composite Catalysts. *Chem. Eng. Process.* **2015**, *97*, 112−133.
(31) Liu, Z.; Sun, D. D.; Guo, P.; Leckie, J. O. An Efficient Bicomponent TiO2/SnO2 Nanofiber Photocatalyst Fabricated by Electrospinning with a Side-by-Side Dual Spinneret Method. *Nano Lett.* **2007**, *7*, 1081−1085.
(32) Khan, M. M.; Adil, S. F.; Al-Mayouf, A. Metal Oxides as Photocatalysts. *J. Saudi Chem. Soc.* **2015**, *19*, 462−464.
(33) Wang, X.; Li, Z.; Shi, J.; Yu, Y. One-Dimensional Titanium Dioxide Nanomaterials: Nanowires, Nanorods, and Nanobelts. *Chem. Rev.* **2014**, *114*, 9346−9384.
(34) Kiran, K. S.; Ashwath Narayana, B. S.; Lokesh, S. V. Enhanced Photocatalytic Activity of Perovskite SrTiO3 Nanorods. *Solid State Technol.* **2020**, *63*, 1913−1920.
(35) Sun, H.; Deng, J.; Qiu, L.; Fang, X.; Peng, H. Recent Progress in Solar Cells Based on One-Dimensional Nanomaterials. *Energy Environ. Sci.* **2015**, *8*, 1139−1159.
(36) Sun, Y.; Liu, N.; Cui, Y. Promises and Challenges of Nanomaterials for Lithium-Based Rechargeable Batteries. *Nat. Energy* **2016**, *1*, 16071.
(37) Yu, Z.; Tetard, L.; Zhai, L.; Thomas, J. Supercapacitor Electrode Materials: Nanostructures from 0 to 3 Dimensions. *Energy Environ. Sci.* **2015**, *8*, 702−730.
(38) Bao, N.; Feng, X.; Shen, L.; Lu, X. Calcination Syntheses of a Series of Potassium Titanates and Their Morphologic Evolution. *Cryst. Growth Des.* **2002**, *2*, 437−442.
(39) Zhang, X.; Tang, S.; Zhai, L.; Yu, J.; Shi, Y.; Du, Y. A Simple Molten Salt Method to Synthesize Single-Crystalline Potassium Titanate Nanobelts. *Mater. Lett.* **2009**, *63*, 887−889.
(40) Banerjee, A. N.; Anitha, V. C.; Joo, S. W. Improved Electrochemical Properties of Morphology-Controlled Titania/Titanate Nanostructures Prepared by in-Situ Hydrothermal Surface Modification of Self-Source Ti Substrate for High-Performance Supercapacitors. *Sci. Rep.* **2017**, *7*, 13227.
(41) Wei, W.; Lü, X.; Jiang, D.; Yan, Z.; Chen, M.; Xie, J. A Novel Route for Synthesis of UV-Resistant Hydrophobic Titania-Containing Silica Aerogels by Using Potassium Titanate as Precursor. *Dalton Trans.* **2014**, *43*, 9456−9467.
(42) Dhandole, L. K.; Ryu, J.; Lim, J.-M.; Oh, B.-T.; Park, J. H.; Kim, B.-G.; Jang, J. S. Hydrothermal synthesis of titanate nanotubes from TiO2 nanorods prepared via a molten salt flux method as an effective adsorbent for strontium ion recovery. *RSC Adv.* **2016**, *6*, 98449−98456.
(43) Kolen'ko, Y. V.; Kovnir, K. A.; Gavrilov, A. I.; Garshev, A. V.; Frantti, J.; Lebedev, O. I.; Churagulov, B. R.; Van Tendeloo, G.; Yoshimura, M. Hydrothermal Synthesis and Characterization of Nanorods of Various Titanates and Titanium Dioxide. *J. Phys. Chem. B* **2006**, *110*, 4030−4038.
(44) Cao, J.; Wang, A.; Yin, H.; Shen, L.; Ren, M.; Han, S.; Shen, Y.; Yu, L.; Jiang, T. Selective Synthesis of Potassium Titanate Whiskers Starting from Metatitanic Acid and Potassium Carbonate. *Ind. Eng. Chem. Res.* **2010**, *49*, 9128−9134.
(45) Gulledge, H. Fibrous Potassium Titanate-A New High Temperature Insulating Material. *Ind. Eng. Chem.* **1960**, *52*, 117−118.
(46) He, M.; Lu, X.-H.; Feng, X.; Yu, L.; Yang, Z.-H. A Simple Approach to Mesoporous Fibrous Titania from Potassium Dititanate. *Chem. Commun.* **2004**, 2202−2203.
(47) Leng, M.; Chen, Y.; Xue, J. Synthesis of TiO2 nanosheets via an exfoliation route assisted by a surfactant. *Nanoscale* **2014**, *6*, 8531−8534.
(48) Hirata, T.; Ishioka, K.; Kitajima, M. Vibrational Spectroscopy and X-Ray Diffraction of Perovskite Compounds Sr1−xMxTiO3(M= Ca, Mg; 0 ≤x≤ 1). *J. Solid State Chem.* **1996**, *124*, 353−359.
(49) Song, Y.; Luo, M.; Zhao, D.; Peng, G.; Lin, C.; Ye, N. Explorations of new UV nonlinear optical materials in the Na2CO3-CaCO3system. *J. Mater. Chem. C* **2017**, *5*, 8758−8764.
(50) Surya, S. G.; Ashwath, B. S. N.; Mishra, S.; Karthik, A. R. B.; Sastry, A. B.; Prasad, B. L. V.; Rangappa, D.; Rao, V. R. H2S Detection Using Low-Cost SnO2 Nano-Particle Bi-Layer OFETs. *Sens. Actuators, B* **2016**, *235*, 378−385.
(51) Wang, Q.; Zhang, B.; Lu, X.; Zhang, X.; Zhu, H.; Li, B. Multifunctional 3D K2Ti6O13 nanobelt-built architectures towards wastewater remediation: selective adsorption, photodegradation, mechanism insight and photoelectrochemical investigation. *Catal. Sci. Technol.* **2018**, *8*, 6180−6195.
(52) Veldurthi, N. K.; Velchuri, R.; Pola, S.; Prasad, G.; Muniratnam, N. R.; Vithal, M. Synthesis, Characterization and Silver/Copper-Nitrogen Substitutional Effect on Visible Light Driven Photocatalytic Performance of Sodium Hexatitanate Nanostructures. *J. Chem. Technol. Biotechnol.* **2015**, *90*, 1507−1514.

https://dx.doi.org/10.1021/acsomega.0c02087
ACS Omega 2021, 6, 7248−7256